Calculation of the Redox Properties of Aromatics and Prediction of Their Coupling Mechanism and Oligomer Redox Properties

John B. Henry and Andrew R. Mount*

School of Chemistry, The University of Edinburgh, King's Buildings, West Mains Road, Edinburgh EH9 3JJ, United Kingdom

Received: August 12, 2009; Revised Manuscript Received: September 15, 2009

The B3LYP density functional theory method has been used to determine theoretical values for the peak oxidation potentials for a range of redox-active aromatics in acetonitrile at room temperature. Excellent agreement to within 37 mV is found between these values and those observed experimentally. The calculated electron spin density distributions of indole monomer and indole oligomer radical cations also enable a plausible mechanism to be advanced by which the experimentally observed asymmetric trimer product is formed. Theoretical values for the peak oxidation potential of the indole trimer also show excellent agreement with those observed previously in electrochemical studies, again consistent with this asymmetric trimer product. Together, with the previously demonstrated ability of this approach to predict the coupling mechanisms and redox properties of the oligomers formed from indolocarbazole, these calculations provide a method for the in silico screening of molecular properties to inform molecular materials design and electrosynthesis.

Introduction

Quantum mechanical methods such as those based on density functional theory (DFT) are being increasingly utilized for the study of the structure and properties of molecular aromatic systems. For example, DFT has been used to model the solvatochromic effects on absorption and emission[1] and to aid in solution[2] and powder[3] NMR structural characterization. The electrochemical behavior of aromatic molecules such as monomers, conjugated oligomers, and polymers originates from their chemical and electronic structures and properties and is crucial in determining materials properties for a variety of applications across chemistry, physics, and biology such as (bio)sensors, organic electronic devices, supercapacitors, and electroluminescent films.[4] With increased computational power now locally available through computational cluster facilities, DFT can now be used to calculate the molecular electronic properties of these larger aromatic systems. The establishment of accurate calculation methods should make possible the in silico screening of molecular properties to assess their applicability, particularly for electroactive materials applications, prior to synthesis.

In this study, DFT was first been used to determine the peak oxidation potentials of a range of redox-active aromatic molecules (Figure 1). Through comparison with experiment, this establishes much enhanced accuracy for these calculations over those reported previously[5−7] for organic systems. Given the demonstrated effectiveness of this method in predicting the coupling products of indolocarbazole electrooxidation,[8] we have also probed its applicability to the prediction of the nature and properties of the coupling product(s) of another aromatic: indole. The motivation is 3-fold: First, 5-substituted indoles present an interesting class of heteroaromatics. Electrooxidation has been shown to form highly conducting electroactive films, of potential interest in a variety of materials applications, including fast-response pH sensors,[9] bioactive electrodes,[10,11] and cathodes in aqueous rechargeable cells.[12] Second, they have been studied extensively, and the monomer is well-characterized experimentally, which is invaluable for calculation validation. Third, the coupling mechanism of 5-substituted indoles for film formation and the nature of the oligomeric products is still a subject of some debate in the literature. Despite the full characterization of the electrooxidation product as an asymmetric cyclic trimer (Figure 1h) by a combination of NMR spectroscopy and electrochemical methods,[13−15] some groups still postulate the formation under certain conditions of a linear polymeric product with a regular indole 2,3-linkage. We have therefore used our DFT calculations to give insight into the coupling reaction, to produce a plausible mechanism for asymmetric trimer formation, to address the likelihood of linear 2,3-polymer formation, and to establish whether such techniques can be applied more generally to redox-active aromatic systems.

Calculation of Redox Potentials. Accurate calculation of redox potentials is essential first for in silico method validation through comparison with experimental values and second for the rational design and screening of novel redox molecular systems prior to synthesis through prediction of their thermodynamic properties.[19] As well as general calculations on a range of organic[6,7,20,21] and inorganic[20,22,23] systems, previous work has mainly focused on biologically important molecules (such as quinones[24−26] or DNA base analogues[27]) and environmentally important systems (such as hexachloroethane[28] and anilines[29]). Studies[5,26] have typically shown that the calculation of redox potentials using DFT provides greater accuracy than semiempirical methods. For example, Baik and Friesner[20] found that reasonable accuracy was achievable for organic molecules, whereas metallocenes and a range of simple ligand systems gave systematic deviations of calculated from experimental values of more than 100 mV. This suggests that the large error observed by Kettle et al.[5] is at least partly due to a systematic error in the calculation of the metallocene reduction potential. Fu et al. calculated the redox potentials of roughly 270 structurally unrelated organic molecules in both implicit acetonitrile[6] and dimethyl sulfoxide (DMSO)[7] solvent and found a large overall standard deviation compared to experimental values of 170 mV

* To whom correspondence should be addressed. E-mail: A.Mount@ed.ac.uk.

10.1021/jp907792b CCC: $40.75
Published on Web 10/02/2009

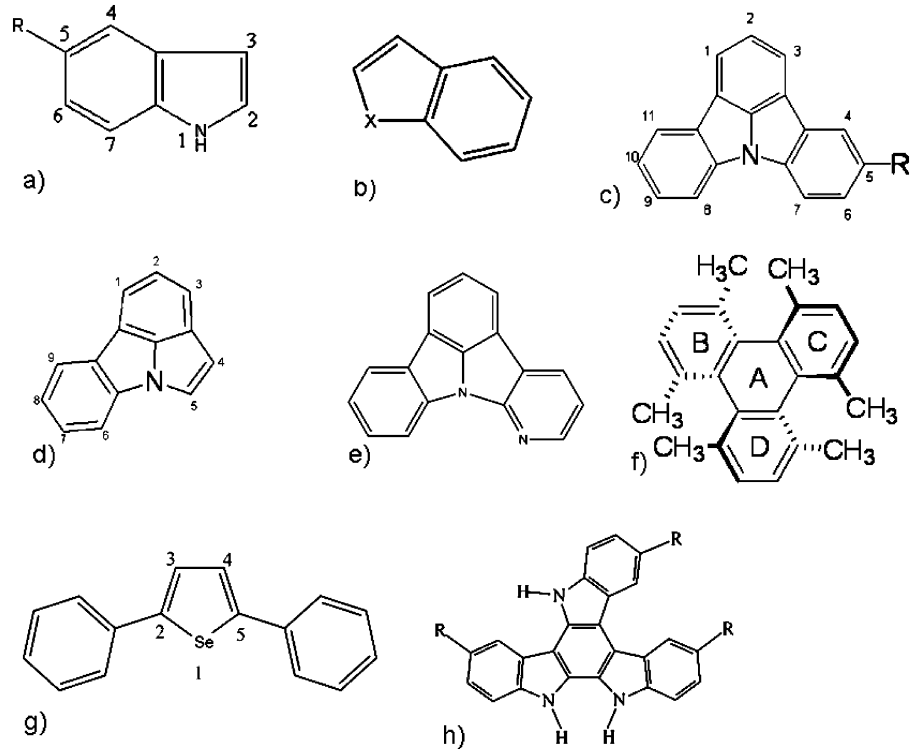

Figure 1. Structures of the (a) 5-substituted indoles (R = H, CH_3, Br, CO_2H, Cl, OCH_3, NO_2, NH_2, OH, CN), (b) indole analogues (X = O, S, Se), (c) 5-substituted indolo(3,2,1-*jk*)carbazoles (R = H,[8] CH_3, Br, NH_2, CN), (d) pyrrolo(3,2,1-*jk*)carbazole,[16] (e) 7-azaindolo(3,2,1-*jk*)carbazole, (f) 1,4,5,8,9,12-hexamethyltriphenylene,[17] (g) dibenzoselenophene,[18] and (h) the asymmetric cyclic trimer product formed on electrooxidation of (a).

in acetonitrile and 110 mV in DMSO. Such errors preclude the accurate screening of systems for redox properties.

For electron transfer reactions, the calculation of the free energy of an electron in a metal electrode is fraught with difficulty. Intensive computational methods have been employed to model electron transfer from electrodes to ions;[30] such techniques are, however, highly computationally expensive. In general, the standard approach is therefore to calculate the absolute electrode potential for the redox reaction of the molecular species of interest and subtract from it the absolute electrode potential of a reference redox couple which forms the basis of a common reference electrode such as the saturated calomel electrode (SCE) or the standard or normal hydrogen electrode (SHE or NHE).[31] Although absolute potentials for these reference electrode reactions have been calculated and are reported in the literature, caution should be exercised when using this approach as there is little agreement on their values, reflecting the difficulty of their calculation; Namazian and Coote quote a value of −4.52 V for the SHE, quoting the paper by Kelly et al.,[32] which reports that the value of −4.52 V relates to the NHE, while the calculation of oxidation potentials in acetonitrile by Fu et al.[6] uses a value of −4.44 V for the NHE, although this relates to the absolute electrode potential of the NHE in aqueous solution.[31] Applying this value to acetonitrile solutions completely neglects the liquid-junction and solvation effects that would be present, and Trasatti recommends a value of −4.60 ± 0.10 V for the NHE in acetonitrile.[31] It should be noted that this gives a minimum error in reduction potentials calculated using this value of 100 mV. Avoiding this use of absolute electrode potentials for standard reference electrodes, the approach in this work is to calculate directly the reduction potential difference between the redox system of interest, $X^{\bullet+}$/X, and another (reference) redox system, $Y^{\bullet+}$/Y. The standard reduction potential, $E°$, is then calculated from the following reaction:[5,26]

$$X^{\bullet+} + Y \xrightarrow{\Delta G°} X + Y^{\bullet+}$$

where

$$\Delta G° = \Delta G_X° - \Delta G_Y° = -F[E_X° - E_Y°] = -FE° \quad (1)$$

The general approach to calculating the standard free energy change, $\Delta G°$, is to first compute gas-phase ionization energies for the molecular species and then correct for the solvation energy (using in our case implicit PCM solvation) and temperature (by performing a frequency calculation) on each optimized structure. For assessment of the accuracy of these calculations, $E°$ is then compared to that calculated from the difference between the experimental values of $E_X°$ and $E_Y°$, measured with respect to a common reference electrode. In this work, we have chosen unsubstituted indole as Y to reduce systematic error. Conversion of these values to the standard ferrocene/ferrocinium (Fc/Fc^+) reference scale has been achieved by measuring the experimental indole oxidation potential with respect to Fc/Fc^+ and subtracting this value from $E°$.

While using this approach, caution should be exercised when converting experimental potentials obtained or calculated with one reference electrode to another reference scale using literature values, due to variability in stated experimental reference potentials.[33]

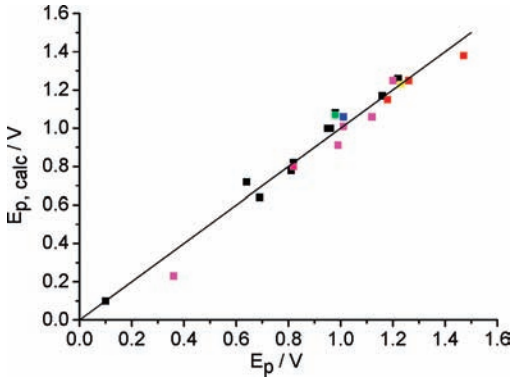

Figure 2. Calculated, $E_{p,calc}$, vs measured, E_p, peak oxidation potentials of (black) 5-substituted indoles, (red) indole analogues, (purple) 5-substituted indolo(3,2,1-*jk*)carbazoles, (green) pyrrolo(3,2,1-*jk*)carbazole, (yellow) 7-azaindolo(3,2,1-*jk*)carbazole, (blue) 1,4,5,8,9,12-hexamethyltriphenylene, and (pink) dibenzoselenophene. The line shows the ideal relationship if calculated and experimental data are identical.

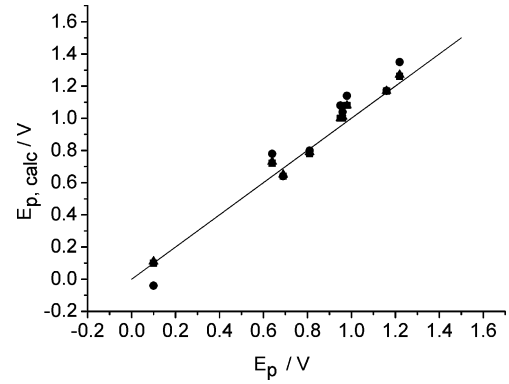

Figure 3. Calculated, $E_{p,calc}$, vs measured, E_p, peak oxidation potentials of substituted indole monomers with basis sets (■) 6-311+G(d,p) with temperature corrections, (▲) 6-311+G(d,p) without temperature correction, and (●) 6-31G with temperature correction. The line shows the ideal relationship if calculated and experimental data are identical.

Comparison of Calculated and Experimental Data. For those species such as indole monomers which display chemically irreversible oxidation peaks due to chemical coupling, it can often be difficult to establish a precise experimental value of $E°$.[6] It is, however, possible to determine $E°$ from the measured peak potential for electrochemically reversible systems. A test of electrochemical reversibility which can still be applied when there is chemical irreversibility on oxidation is the separation of the peak potential, E_p, and the half-peak potential, $E_{p/2}$, as $|E_p - E_{p/2}| = 57$ mV for a 1-electron reversible redox reaction at 298 K.[34] For example, the measured value of $E_p - E_{p/2}$ for unsubstituted 1 mM indole oxidation in acetonitrile, uncompensated for *iR* drop, was found to be 63 mV at a sweep rate of 100 mV s^{-1} and 57 mV when compensating for *iR* drop; similar results were found for all the aromatics studied, suggesting that the assumption of electrochemical reversibility is reasonable. In this case, $E°$ is readily related to $E_{p/2}$ through

$$E_{p/2} = E° + \frac{RT}{F}\left(1.09 + \ln\left(\frac{D_O}{D_R}\right)^{1/2}\right) \qquad (2)$$

where D_O and D_R are the diffusion coefficients of the reduced and oxidized species, respectively.[34] Often for aromatics with extensive electronic conjugation, $D_O \approx D_R$, which removes the second term in parentheses in eq 2.

As both $X/X^{\bullet+}$ and $Y/Y^{\bullet+}$ reactions satisfy the criteria for electrochemical reversibility, $E°$ is also therefore the peak oxidation potential of X with respect to the peak oxidation potential of Y.

Results and Discussion

Calculation of Oxidation Potentials. The peak oxidation potentials of the 20 heteroaromatic and 1 aromatic molecules (Figure 1) have been calculated using the B3LYP method and 6-311+G(d,p) basis set with temperature correction given by frequency calculations. Figure 2 shows these data compared with experimentally measured values. There is close agreement between experiment and theory for all molecules, with a root-mean-square error (RMSE) of 37 mV, demonstrating the relative accuracy of these calculations for this wide variety of redox-active aromatics and the efficacy of using indole as the standard. Given the differences in aromatic structure, including changes in the presence and nature of heteroatoms, and the propensity for specific solvent interaction through, e.g., NH functional groups, it is satisfying that the implicit solvation model utilized in these calculation can achieve this accuracy while avoiding the need for specific solvation; this allows calculations of oligomeric properties.

It is, however, not surprising that calculations on the subset of 5-substituted indoles (for which both X and Y have the same aromatic functionality and for which the effects of specific solvation should largely cancel) show a smaller overall error. Figure 3 shows calculations of E_p for the 5-substituted indoles using the B3LYP method with both the relatively small 6-31G and the extended 6-311+G(d,p) basis sets (tabulated in Table S1, Supporting Information). These small and larger basis sets can be seen to provide a reasonable route to the calculation of oxidation potentials, with the larger basis set giving an RMSE of 31 mV. With the smaller basis set the RMSE is 59 mV, but these calculations are up to 9 times shorter to run. The effects of temperature correction largely cancel for these data when calculating redox potentials; temperature-corrected calculations give a standard deviation of 31 mV compared to 32 mV without temperature correction. This demonstrates that these Gaussian 03 calculations can readily calculate oxidation potentials to an accuracy of a few tens of millivolts.

Coupling Mechanism of 5-Substituted Indoles. This relatively simple computational method enables calculations on larger aromatic systems, which allows the nature and properties of oligomeric products formed by monomer electrooxidation and coupling to now be addressed. For a variety of heteroaromatics,[35] coupling has previously been shown to occur through coupling of monomer radical cations.[15] It has been argued that the most likely coupling sites are those with the highest electron spin density where there will be the highest propensity for radical−radical coupling and bond formation.[5,36] We have previously shown for unsubstituted indolo(3,2,1-*jk*)carbazole[8] that consideration of the radical cation electron spin density results in the successful prediction of the monomer coupling positions and the structure of the resulting dimers. We now extend this approach to the electrooxidation and coupling of indole, whose product is a trimer. As previously shown by Kettle et al.,[5] the monomer radical spin density distributions (Figure 4) give a pictorial representation of the location of the radical spin (the unpaired electron), with similar spin density distributions for all except amino and hydroxy (Figure 4e,f), for which greater spin density is located on or near the substituent. For

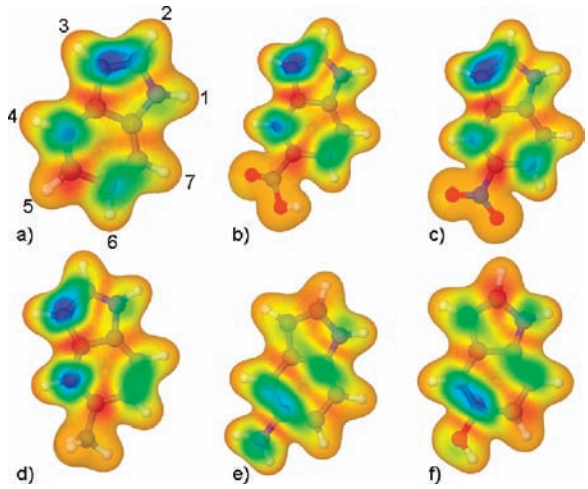

Figure 4. Spin density distribution mapped onto a 99% electron density isosurface for the radical cations of (a) indole (with ring numbering indicated), (b) indole-5-carboxylic acid, (c) 5-nitroindole, (d) 5-methylindole, (e) 5-aminoindole, and (f) 5-hydroxyindole. (The coloring scheme is roygb: blue indicates a positive spin density (0.005), while red is negative (−0.001). The same spin density scale was used for all maps.)

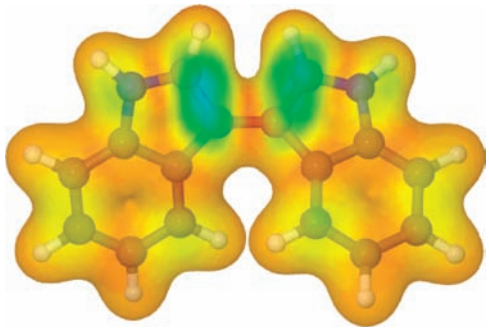

Figure 5. Spin density distribution mapped onto a 99% electron density isosurface for the radical cation of the 3,3′-indole dimer.

indole (Figure 4a) the greatest electron spin density is found on the 3-position of the indole. Coupling of two monomer radical cations with the loss of 2 protons would therefore be expected to yield the 3,3′-coupled indole dimer species shown in Figure 5.

The peak oxidation potential of the 3,3′-unsubstituted resulting indole dimer was then calculated using B3LYP/6-311+G(d,p) to be -0.11 ± 0.03 V vs Fc^+/Fc. This means the electrode potential used is more than sufficient to oxidize indole dimer upon formation.[15] (Given the similarity in the molecular structure, we suggest the error in the dimer oxidation potential is likely to be comparable with that of the calculated monomer peak oxidation potentials. However, even if it were larger, this value would still be much lower than the experimental indole monomer peak oxidation potential (+0.820 V vs Fc^+/Fc).) In previous electrochemical experiments this oxidized dimer intermediate was never detected at a ring electrode, despite this suitable redox potential and the expectation of dimer solubility, which suggests its concentration is low due to further rapid coupling.[15] The most likely coupling is therefore between the radical cation of this dimer and that of a monomer. Figure 5 shows the spin density distribution for the resulting 3,3′-dimer radical cation. It can be seen that the greatest spin density can be observed in the 2- and 2′-positions at the top of the molecule as shown; therefore, we argue any unreacted indole monomer radical in close proximity to the oxidized dimer is likely to

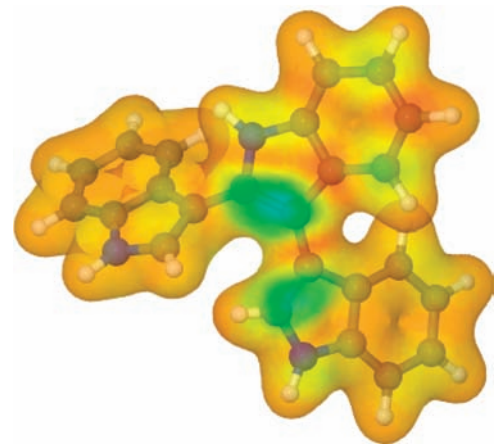

Figure 6. Spin density distribution mapped onto a 99% electron density isosurface for the radical cation of the suggested linear indole trimer intermediate.

undergo coupling via one of the equivalent 2-positions on the monomers which make up this dimer and the 3-position on the monomer to form the linear trimer species shown in Figure 6.

Calculations have also been performed on the neutral and radical cation forms of this linear trimer using B3LYP/6-31G; the smaller basis set is required due to the large number of atoms in this system. The calculated oxidation potential was found to be 0.12 ± 0.06 V vs Fc^+/Fc, where the stated standard deviation again assumes an error similar to that of indole monomer calculations. This is again a much lower potential than the oxidation potential applied to the electrode to induce indole monomer electrooxidation. Once formed, this trimer would, therefore, again be expected to oxidize readily at the electrode surface. The calculated electron spin density for the resulting trimer radical cation is shown in Figure 6. It is interesting to note that the highest electron spin density is now located on only one of the unlinked indole monomer 2-positions, which is consistent with the lack of symmetry in this linear trimer. The site of highest radical spin density is most favored for cyclization and central aromatic ring formation. This would readily lead to formation of the observed asymmetric cyclic trimer product, Figure 9a, we suggest through radical−neutral C−C coupling, proton elimination, and the thermodynamic drive to central ring formation and aromatization through further oxidation. Together, this offers a mechanism for the selective formation of the asymmetric trimer product observed and fully characterized in previous experiments.[13−15]

Redox Properties of Asymmetric Cyclic Trimers of Indole. Previously through rotating ring−disk electrode studies the redox properties of the indole oxidation product have been observed and attributed to the sparingly soluble asymmetric indole trimer species.[15] Having established a plausible mechanistic route to trimer product formation, we have also calculated their peak oxidation potentials (see Table S3, Supporting Information). These show good correspondence with experimental data (Figure 7), reproducing all the observed experimental values to within twice the RMSE (calculated as 83 mV for the 6-31G basis set and 62 mV for the larger 6-311+G basis set), and all but the H and CN substituents to within the overall RMSE (in fact, the experimental value for 5-cyanoindole has been reported as a lower limit, due to practical difficulties with its accurate measurement, which would explain the relatively large error).[15] This confirms that this previously measured product of indole electrooxidation is most likely to be the asymmetric cyclic trimer in all cases.

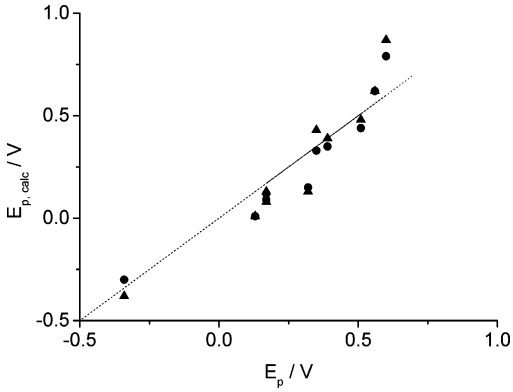

Figure 7. B3LYP-calculated, $E_{p,calc}$, vs experimental, E_p, peak oxidation potentials of asymmetric indole trimers with basis sets (▲) 6-311+G(d,p) without temperature correction and (●) 6-31G with temperature correction. The line corresponds to identical calculated and experimental data.

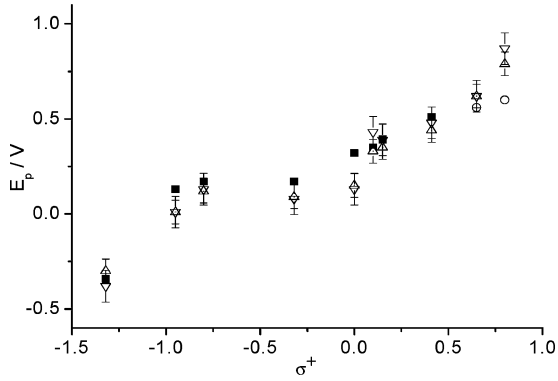

Figure 8. Peak oxidation potentials for 5-substituted indole trimers vs the Hammett substituent parameter, σ^+: (■) experimental[15] and B3LYP-calculated oxidation potentials of indole asymmetric trimers with basis sets (△) 6-311+G(d,p) without temperature correction and (▽) 6-31G with temperature correction. (The experimental values for 5-nitroindole and 5-cyanoindole (○) are lower limits for the experimental peak oxidation potentials.[15])

It can also be seen (Figure 8) that these calculated oxidation potentials reproduce the observed essentially linear relationship with the Hammett substituent parameter previously observed experimentally, including the systematic deviation of the −OX substituents from this line.[15] This suggests this offset arises from differences in the electronic structures of these trimer species, with −OX substitution not conforming to the simple Hammett picture of substituent perturbation of a common aromatic core, and not as a result of solution aggregation as previously suggested.[15]

The electron spin density map for selected asymmetric cyclic trimers is shown in Figure 9. It is clear for all trimers that the majority of this radical electron density is located on the central benzene ring, where coupling is precluded; this may explain why this 1+ state of the formed trimer films is chemically stable, the 0/1+ redox reaction is electrochemically reversible, and coupling of trimer centers occurs only upon further oxidation.[14] Interestingly, the variation in radical cation spin density distribution with substituent appears much smaller for these trimers than for the monomers, despite the fact that there is a similar experimental and calculated deviation of the peak oxidation potential from the Hammett relationship for these −OX substituents.

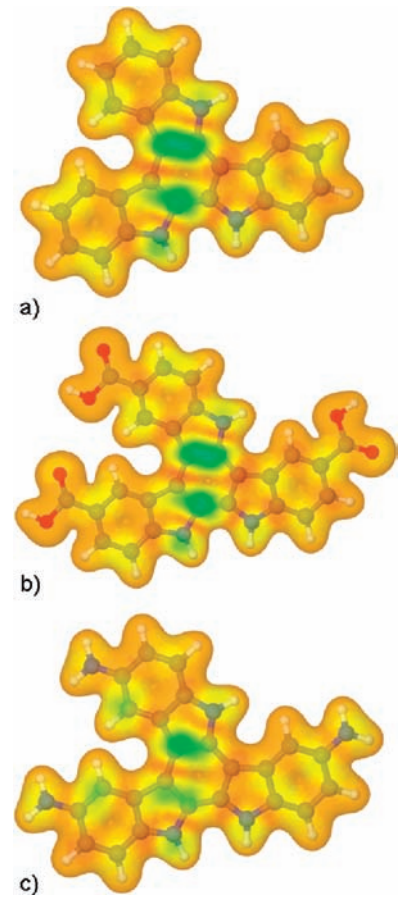

Figure 9. Spin density distribution mapped onto a 99% electron density isosurface for the radical cation of the asymmetric (a) indole, (b) indole-5-carboxylic acid, and (c) 5-aminoindole trimer products of electrooxidation.

Conclusions

The results presented in this paper have shown that DFT calculations of the energies of neutral and radical cationic forms of a wide range of aromatics can be used to determine peak oxidation potentials which are in close agreement with experimentally measured values. Furthermore, through consideration of the radical density distribution in indole monomer, dimer, and linear trimer radical cations, a plausible mechanism of electrooxidation and coupling can be deduced which explains the formation of the asymmetric trimer product. Calculation of the peak oxidation potentials of this predicted product for asymmetric trimers also gives good agreement with previously measured electrochemical redox potentials. In combination with the previously reported spectroscopic data, this confirms that the product of indole electrooxidation is the asymmetric linked trimer, and not the polymer with regular 2,3-linkages postulated by others; in fact, as the initial coupling product is most likely to be the 3,3′-dimer, it is hard to see how a regular 2,3-polymer can be produced under any conditions without significant intermolecular rearrangement of the aromatic framework. The justification for the formation of a 2,3-linked polymer is the absence of peaks from the C−H bonds in the indole 2- and 3-positions in IR spectra and 1-D NMR spectra.[37−39] However, this observation is also entirely consistent with and explicable by asymmetric trimer formation, and this work suggests a 2,3-linear polymer is not formed under these conditions. This work also suggests there may be a real prospect of selective indole dimer coupling through dimer synthesis followed by electrooxidative coupling in the absence of monomer radical cations (e.g.,

by the use of relatively low potential selective dimer oxidation) to yield tetramers and other novel extended aromatic structures. This is a focus of further experimental and theoretical study.

As this method has also recently been employed for the accurate calculation of the redox properties and coupling characteristics of the indolocarbazole[8] and hexamethlytriphenylene[17] systems, this suggests its potential in the screening of a variety of similar extended heteroaromatic systems for redox and coupling properties.

Experimental Section

All calculations were carried out using the software package Gaussian 03[40] running on an SUSe 9.x Linux HPC cluster consisting of 68 AMD Opteron processing cores contained within the EaStChem Research Computing Facility Hare cluster. Default convergence criteria were used for all calculations (maximum force 0.00045, rms force 0.0003, maximum displacement 0.0018, and rms displacement 0.0012). The computational method employed was B3LYP, the Becke[41] three-parameter hybrid functional which utilizes the correlation functional of Lee, Yang, and Parr[42] and includes both local and nonlocal terms. For calculations of the electron spin density the unrestricted method uB3LYP was employed. The basis set used in all calculations was 6-311+G(d,p) with acetonitrile solvation modeled with the polarizable continuum model (PCM);[43] the parameters used for the solvation model are the Gaussian defaults.[40]

For all molecules a frequency calculation was performed with optimized geometries to ensure that a minimum in the potential energy hypersurface had been reached and to obtain temperature-corrected free energies for the molecules at 298 K.

The spin density distribution was evaluated by generating cube files for electron density and electron spin from the solution calculations. The spin density distribution plots were then made by mapping onto the 99% electron density surface. Output was viewed using Jmol, an open-source Java viewer for chemical structures in 3D (http://www.jmol.org/) and rendered using the Persistence of Vision Raytracer freeware (http://www.povray.org).

Acknowledgment. J.B.H. thanks the School of Chemistry, The University of Edinburgh, for funding. This work has made use of the resources provided by the EaStCHEM Research Computing Facility (http://www.eastchem.ac.uk/rcf). This facility is partially supported by the eDIKT initiative (http://www.edikt.org). The School of Chemistry is part of the EaStCHEM joint Chemistry Research School. We acknowledge the financial support of the Scottish Funding Council.

Supporting Information Available: Tables of experimentally measured and calculated peak oxidation potentials for Figures 3, 4, and 8 and complete reference details for ref 40. This material is available free of charge via the Internet at http://pubs.acs.org.

References and Notes

(1) Han, W.-G.; Liu, T.; Himo, F.; Toutchkine, A.; Bashford, D.; Hahn, K. M.; Noodleman, L. *ChemPhysChem* **2003**, *4*, 1084–1094.

(2) Tait, K. M.; Parkinson, J. A.; Gibson, D. I.; Richardson, P. R.; Ebenezer, W. J.; Hutchings, M. G.; Jones, A. C. *Photochem. Photobiol. Sci.* **2007**, *6*, 1010–1018.

(3) Pickard, C. J.; Salagar, E.; Pintacuda, G.; Elena, B.; Emsley, L. *J. Am. Chem. Soc.* **2007**, *129*, 8932–8933.

(4) Boudreault, P. L. T.; Wakim, S.; Blouin, N.; Simard, M.; Tessier, C.; Tao, Y.; Leclerc, M. *J. Am. Chem. Soc.* **2007**, *129*, 9125–9136.

(5) Kettle, L. J.; Bates, S. P.; Mount, A. R. *Phys. Chem. Chem. Phys.* **2000**, *2*, 195–201.

(6) Fu, Y.; Liu, L.; Yu, H.-Z.; Wang, Y.-M.; Guo, Q.-X. *J. Am. Chem. Soc.* **2005**, *127*, 7227–7234.

(7) Fu, Y.; Liu, L.; Wang, Y.-M.; Li, J.-N.; Yu, T.-Q.; Guo, Q.-X. *J. Phys. Chem. A* **2006**, *110*, 5874–5886.

(8) Wharton, S. I.; Henry, J. B.; McNab, H.; Mount, A. R. *Chem.—Eur. J.* **2009**, *15*, 5482–5490.

(9) Bartlett, P. N.; Farrington, J. *Bull. Electrochem.* **1992**, *8*, 208–211.

(10) Bartlett, P. N.; Farrington, J. *J. Electroanal. Chem.* **1989**, *261*, 471–475.

(11) Biegunski, A. T.; Michoti, A.; Bukowska, J.; Jackowska, K. *Bioelectrochemistry* **2005**, *69*, 41–48.

(12) Sivakkumar, S. R.; Angulakshmi, N.; Saraswathi, R. J. *J. Appl. Polym. Sci.* **2005**, *98*, 917–922.

(13) Mackintosh, J. G.; Mount, A. R.; Reed, D. *Magn. Reson. Chem.* **1994**, *32*, 559–561.

(14) Mackintosh, J. G.; Redpath, C. R.; Jones, A. C.; Langridge-Smith, P. R. R.; Mount, A. R. *J. Electroanal. Chem.* **1995**, *388*, 179–185.

(15) Jennings, P.; Jones, A. C.; Mount, A. R.; Thomson, A. D. *J. Chem. Soc., Faraday Trans.* **1997**, *93*, 3791–3797.

(16) Crawford, L. A.; McNab, H.; Mount, A. R.; Wharton, S. I. *J. Org. Chem.* **2008**, *73*, 6642–6646.

(17) Wang, Y.; Stretton, A. D.; McConnell, M. C.; Wood, P. A.; Parsons, S.; Henry, J. B.; Mount, A. R.; Galow, T. H. *J. Am. Chem. Soc.* **2007**, *129*, 13193–13200.

(18) Hua, G.; Li, Y.; Slawin, A. M. Z.; Woollins, J. D.; Henry, J. B.; Mount, A. R. Manuscript in preparation.

(19) Reynolds, C. A.; King, P. M.; Richards, W. G. *Nature* **1988**, *334*, 80–82.

(20) Baik, M.-H.; Friesner, R. A. *J. Phys. Chem. A* **2002**, *106*, 7407–7412.

(21) Charles-Nicolas, O.; Lacroix, J. C.; Lacaze, P. C. *J. Chim. Phys. Phys.-Chim. Biol.* **1998**, *95*, 1457–1460.

(22) Uedsemaa, M.; Tamm, T. *J. Phys. Chem. A* **2003**, *107*, 9997–10003.

(23) Qi, X.-J.; Fu, Y.; Liu, L.; Guo, Q.-X. *Organometallics* **2007**, *26*, 4197–4203.

(24) Raymond, K. S.; Grafton, A. K.; Wheeler, R. A. *J. Phys. Chem. B* **1997**, *101*, 623–631.

(25) Namazian, M.; Norouzi, P.; Ranjbar, R. *J. Mol. Struct.: THEOCHEM* **2003**, *625*, 235–241.

(26) Namazian, M. *J. Mol. Struct.: THEOCHEM* **2003**, *664−665*, 273–278.

(27) Baik, M.-H.; Silverman, J. S.; Yang, I. V.; Ropp, P. A.; Szalai, V. A.; Yang, W.; Thorp, H. H. *J. Phys. Chem. B* **2001**, *105*, 6437–6444.

(28) Patterson, E. V.; Cramer, C. J.; Truhlar, D. G. *J. Am. Chem. Soc.* **2001**, *123*, 2025–2031.

(29) Winget, P.; Weber, E. J.; Cramer, C. J.; Truhlar, D. G. *Phys. Chem. Chem. Phys.* **2000**, *2*, 1231–1239.

(30) Reed, S. K.; Madden, P. A.; Papadopoulos, A. *J. Chem. Phys.* **2008**, *128*, 124701–124710.

(31) Trasatti, S. *Pure Appl. Chem.* **1986**, *58*, 955–966.

(32) Kelly, C. P.; Cramer, C. J.; Truhlar, D. G. *J. Phys. Chem. B* **2007**, *111*, 408–422.

(33) Pavlishchuk, V. V.; Addison, A. W. *Inorg. Chim. Acta* **2000**, *298*, 97–102.

(34) Bard, A. J.; Faulkner, L. R. Potential Sweep Methods. *Electrochemical Methods: Fundamentals and Applications*, 2nd ed.; John Wiley & Sons, Inc.: New York, 2001; p 231.

(35) Waltman, R. J.; Bargon, J. *Can. J. Chem.* **1986**, *64*, 76–95.

(36) Waltman, R. J.; Diaz, A. F.; Bargon, J. *J. Phys. Chem.* **1984**, *88*, 4343–4346.

(37) Xu, J.; Hou, J.; Zhou, W.; Nie, G.; Pu, S.; Zhang, S. *Spectrochim. Acta, A* **2006**, *63*, 723–728.

(38) Nie, G.; Cai, T.; Zhang, S.; Bao, Q.; Xu, J. *Electrochim. Acta* **2007**, *52*, 7097–7106.

(39) Kim, S.; Miyagawa, N.; Seki, H.; Ishikawa, T.; Hoshino, K. *J. Electroanal. Chem.* **2008**, *615*, 12–18.

(40) Frisch, M. J.; et al. *Gaussian 03*, revision C.02; Gaussian, Inc.: Wallingford, CT, 2004.

(41) Becke, A. D. *Phys. Rev. A* **1988**, *38*, 3098–3100.

(42) Lee, C.; Yang, W.; Parr, R. G. *Phys. Rev. B* **1988**, *37*, 785–789.

(43) Mennucci, B.; Tomasi, J. *J. Chem. Phys.* **1997**, *106*, 5151–5158.

JP907792B